Research Article | Vol. 26, No. 12 | 11 Jun 2018 | OPTICS EXPRESS 15745

Optics EXPRESS

Chirp-control of resonant high-order harmonic generation in indium ablation plumes driven by intense few-cycle laser pulses

Z. ABDELRAHMAN,[1,6] M. A. KHOKHLOVA,[1,2,6,*] D. J. WALKE,[1] T. WITTING,[3] A. ZAIR,[1,4] V. V. STRELKOV,[2,5] J. P. MARANGOS,[1] AND J. W. G. TISCH[1]

[1]*Blackett Laboratory, Imperial College, London SW7 2AZ, UK*
[2] *A.M. Prokhorov General Physics Institute of the RAS, Moscow 119991, Russia*
[3]*Max Born Institute for Nonlinear Optics and Short Pulse Spectroscopy, Max-Born-Straße 2a, 12489 Berlin, Germany*
[4]*Kings College London, Department of Physics, London WC2R 2LS, UK*
[5]*Moscow Institute of Physics and Technology (State University), 141700 Dolgoprudny, Moscow Region, Russia*
[6]*Contributed equally to this work and are listed alphabetically*
**m.khokhlova@imperial.ac.uk*

Abstract: We have studied high-order harmonic generation (HHG) in an indium ablation plume driven by intense few-cycle laser pulses centered at 775 nm as a function of the frequency chirp of the laser pulse. We found experimentally that resonant emission lines between 19.7 eV and 22.3 eV (close to the 13th and 15th harmonic of the laser) exhibit a strong, asymmetric chirp dependence, with pronounced intensity modulations. The chirp dependence is reproduced by our numerical time-dependent Schrödinger equation simulations of a resonant HHG by the model indium ion. As demonstrated with our separate simulations of HHG within the strong field approximation, the resonance can be understood in terms of the chirp-dependent HHG photon energy coinciding with the energy of an autoionizing state to ground state transition with high oscillator strength. This supports the validity of the general theory of resonant four-step HHG in the few-cycle limit.

OCIS codes: (190.4160) Multiharmonic generation; (270.6620) Strong-field processes; (320.7150) Ultrafast spectroscopy.

References and links

1. R. A. Ganeev, M. Suzuki, M. Baba, H. Kuroda, and T. Ozaki, "Strong resonance enhancement of a single harmonic generated in the extreme ultraviolet range," Opt. Lett. **31**(11), 1699–1701 (2006).
2. R. A. Ganeev, H. Singhal, P. A. Naik, V. Arora, U. Chakravarty, J. A. Chakera, R. A. Khan, I. A. Kulagin, P. V. Redkin, M. Raghuramaiah, and P. D. Gupta, "Harmonic generation from indium-rich plasmas," Phys. Rev. A **74**(6), 063824 (2006).
3. R. A. Ganeev, "Harmonic generation in laser-produced plasmas containing atoms, ions and clusters: a review," J. Mod. Opt. **59**(5), 409–439 (2012).
4. R. A. Ganeev, Z. Abdelrahman, F. Frank, T. Witting, W. A. Okell, D. Fabris, C. Hutchison, J. P. Marangos, and J. W. G. Tisch, "Spatial coherence measurements of non-resonant and resonant high harmonics generated in laser ablation plumes," Appl. Phys. Lett. **104**(2), 021122 (2014).
5. A. Ravasio, D. Gauthier, F. R. N. C. Maia, M. Billon, J.-P. Caumes, D. Garzella, M. Géléoc, O. Gobert, J.-F. Hergott, A.-M. Pena, H. Perez, B. Carré, E. Bourhis, J. Gierak, A. Madouri, D. Mailly, B. Schiedt, M. Fajardo, J. Gautier, P. Zeitoun, P. H. Bucksbaum, J. Hajdu, and H. Merdji, "Single-shot diffractive imaging with a table-top femtosecond soft x-ray laser-harmonics source," Phys. Rev. Lett. **103**(2), 028104 (2009).
6. F. Krausz and M. Ivanov, "Attosecond physics," Rev. Mod. Phys. **81**(1), 163–234 (2009).
7. C. Altucci, J. W. G. Tisch, and R. Velotta, "Single attosecond light pulses from multi-cycle laser sources," J. Mod. Opt. **58**(18), 1585 (2011).
8. V. V. Strelkov, "Attosecond-pulse production using resonantly enhanced high-order harmonics," Phys. Rev. A **94**(6), 063420 (2016).

#326218 https://doi.org/10.1364/OE.26.015745
Journal © 2018 Received 20 Mar 2018; revised 5 May 2018; accepted 7 May 2018; published 7 Jun 2018

Optics EXPRESS

9. R. A. Ganeev, T. Witting, C. Hutchison, F. Frank, M. Tudorovskaya, M. Lein, W. A. Okell, A. Zaïr, J. P. Marangos, and J. W. G. Tisch, "Isolated sub-fs XUV pulse generation in Mn plasma ablation," Opt. Express **20**(23), 25239–25248 (2012).
10. S. Haessler, V. Strelkov, L. B. Elouga Bom, M. Khokhlova, O. Gobert, J.-F. Hergott, F. Lepetit, M. Perdrix, T. Ozaki, and P. Salières, "Phase distortions of attosecond pulses produced by resonance-enhanced high harmonic generation," New J. Phys. **15**(1), 013051 (2013).
11. V. Strelkov, "Role of autoionizing state in resonant high-order harmonic generation and attosecond pulse production," Phys. Rev. Lett. **104**(12), 123901 (2010).
12. P. B. Corkum, "Plasma perspective on strong field multiphoton ionization," Phys. Rev. Lett. **71**(13), 1994–1997 (1993).
13. K. J. Schafer, B. Yang, L. F. DiMauro, and K. C. Kulander, "Above threshold ionization beyond the high harmonic cutoff," Phys. Rev. Lett. **70**(11), 1599–1602 (1993).
14. V. V. Strelkov, M. A. Khokhlova, and N. Y. Shubin, "High-order harmonic generation and Fano resonances," Phys. Rev. A **89**(5), 053833 (2014).
15. F. Calegari, D. Ayuso, A. Trabattoni, L. Belshaw, S. De Camillis, S. Anumula, F. Frassetto, L. Poletto, A. Palacios, P. Decleva, J. B. Greenwood, F. Martín, and M. Nisoli, "Ultrafast electron dynamics in phenylalanine initiated by attosecond pulses," Science **346**(6207), 336–339 (2014).
16. D. Fabris, T. Witting, W. A. Okell, D. J. Walke, P. Matia-Hernando, J. Henkel, T. R. Barillot, M. Lein, J. P. Marangos, and J. W. G. Tisch, "Synchronized pulses generated at 20 eV and 90 eV for attosecond pump–probe experiments," Nat. Photonics **9**(6), 383–387 (2015).
17. A. Baltuška, T. Udem, M. Uiberacker, M. Hentschel, E. Goulielmakis, Ch. Gohle, R. Holzwarth, V. S. Yakovlev, A. Scrinzi, T. W. Hänsch, and F. Krausz, "Attosecond control of electronic processes by intense light fields," Nature **421**(6923), 611–615 (2003).
18. I. J. Sola, E. Mevel, L. Elouga, E. Constant, V. Strelkov, L. Poletto, P. Villoresi, E. Benedetti, J.-P. Caumes, S. Stagira, C. Vozzi, G. Sansone, and M. Nisoli, "Controlling attosecond electron dynamics by phase-stabilized polarization gating," Nat. Phys. **2**(5), 319 (2006).
19. R. A. Ganeev, H. Singhal, P. A. Naik, V. Arora, U. Chakravarty, J. A. Chakera, R. A. Khan, P. V. Redkin, M. Raghuramaiah, and P. D. Gupta, "Single-harmonic enhancement by controlling the chirp of the driving laser pulse during high-order harmonic generation from GaAs plasma," J. Opt. Soc. Am. B **23**(12), 2535 (2006).
20. R. A. Ganeev, C. Hutchison, A. Zaïr, T. Witting, F. Frank, W. A. Okell, J. W. G. Tisch, and J. P. Marangos, "Enhancement of high harmonics from plasmas using two-color pump and chirp variation of 1 kHz Ti:sapphire laser pulses," Opt. Express **20**(1), 90–100 (2012).
21. R. A. Ganeev, V. V. Strelkov, C. Hutchison, A. Zaïr, D. Kilbane, M. A. Khokhlova, and J. P. Marangos, "Experimental and theoretical studies of two-color-pump resonance-induced enhancement of odd and even harmonics from a tin plasma," Phys. Rev. A **85**(2), 023832 (2012).
22. R. A. Ganeev, T. Witting, C. Hutchison, V. V. Strelkov, F. Frank, M. Castillejo, I. Lopez-Quintas, Z. Abdelrahman, J. W. G. Tisch, and J. P. Marangos, "Comparative studies of resonance enhancement of harmonic radiation in indium plasma using multicycle and few-cycle pulses," Phys. Rev. A **88**(3), 033838 (2013).
23. J. S. Robinson, C. A. Haworth, H. Teng, R. A. Smith, J. P. Marangos, and J. W. G. Tisch, "The generation of intense, transform-limited laser pulses with tunable duration from 6 to 30 fs in a differentially pumped hollow fibre," Appl. Phys. B **85**(4), 525–529 (2006).
24. F. Frank, C. Arrell, T. Witting, W. A. Okell, J. McKenna, J. S. Robinson, C. A. Haworth, D. Austin, H. Teng, I. A. Walmsley, J. P. Marangos, and J. W. Tisch, "Invited review article: technology for attosecond science," Rev. Sci. Instrum. **83**(7), 071101 (2012).
25. W. A. Okell, T. Witting, D. Fabris, D. Austin, M. Bocoum, F. Frank, A. Ricci, A. Jullien, D. Walke, J. P. Marangos, R. Lopez-Martens, and J. W. G. Tisch, "Carrier-envelope phase stability of hollow fibers used for high-energy few-cycle pulse generation," Opt. Lett. **38**(19), 3918–3921 (2013).
26. T. Witting, F. Frank, C. A. Arrell, W. A. Okell, J. P. Marangos, and J. W. G. Tisch, "Characterization of high-intensity sub-4-fs laser pulses using spatially encoded spectral shearing interferometry," Opt. Lett. **36**(9), 1680–1682 (2011).
27. C. Hutchison, R. A. Ganeev, T. Witting, F. Frank, W. A. Okell, J. W. G. Tisch, and J. P. Marangos, "Stable generation of high-order harmonics of femtosecond laser radiation from laser produced plasma plumes at 1 kHz pulse repetition rate," Opt. Lett. **37**(11), 2064–2066 (2012).
28. G. Duffy and P. Dunne, "The photoabsorption spectrum of an indium laser produced plasma," J. Phys. At. Mol. Opt. Phys. **34**(6), L173–L178 (2001).
29. I. P. Christov, M. M. Murnane, and H. Kapteyn, "High-harmonic generation of attosecond pulses in the "single-cycle" regime," Phys. Rev. Lett. **78**(7), 1251–1254 (1997).
30. M. Hentschel, R. Kienberger, C. Spielmann, G. A. Reider, N. Milosevic, T. Brabec, P. Corkum, U. Heinzmann, M. Drescher, and F. Krausz, "Attosecond metrology," Nature **414**(6863), 509–513 (2001).
31. M. V. Frolov, N. L. Manakov, A. M. Popov, O. V. Tikhonova, E. A. Volkova, A. A. Silaev, N. V. Vvedenskii, and A. F. Starace, "Analytic theory of high-order-harmonic generation by an intense few-cycle laser pulse," Phys. Rev. A **85**(3), 033416 (2012).
32. W. Holgado, C. Hernández-García, B. Alonso, M. Miranda, F. Silva, L. Plaja, H. Crespo, and I. J. Sola, "Continuous spectra in high-harmonic generation driven by multicycle laser pulses," Phys. Rev. A **93**(1), 013816 (2016).

Optics EXPRESS

33. P. Rudawski, A. Harth, C. Guo, E. Lorek, M. Miranda, C. M. Heyl, E. W. Larsen, J. Ahrens, O. Prochnow, T. Binhammer, U. Morgner, J. Mauritsson, A. L'Huillier, and C. L. Arnold, "Carrier-envelope phase dependent high-order harmonic generation with a high-repetition rate OPCPA-system," Eur. Phys. J. D **69**(3), 70 (2015).
34. G. Sansone, E. Benedetti, J. P. Caumes, S. Stagira, C. Vozzi, M. Nisoli, L. Poletto, P. Villoresi, V. Strelkov, I. Sola, L. B. Elouga, A. Zaïr, E. Mével, and E. Constant, "Shaping of attosecond pulses by phase-stabilized polarization gating," Phys. Rev. A **80**(6), 063837 (2009).
35. M. Lewenstein, P. Balcou, M. Y. Ivanov, A. L'Huillier, and P. B. Corkum, "Theory of high-harmonic generation by low-frequency laser fields," Phys. Rev. A **49**(3), 2117–2132 (1994).
36. E. Pisanty, RB-SFA: "Rotating bicircular high harmonic generation in the strong field approximation," https://github.com/episanty/RB-SFA (2016).
37. A.-T. Le, T. Morishita, and C. D. Lin, "Extraction of the species-dependent dipole amplitude and phase from high-order harmonic spectra in rare-gas atoms," Phys. Rev. A **78**(2), 023814 (2008).
38. M. B. Gaarde, J. L. Tate, and K. J. Schafer, "Macroscopic aspects of attosecond pulse generation," J. Phys. B **41**(13), 132001 (2008).
39. V. V. Strelkov and R. A. Ganeev, "Quasi-phase-matching of high-order harmonics in plasma plumes: theory and experiment," Opt. Express **25**(18), 21068–21083 (2017).

1. Introduction

High-order harmonic generation (HHG) in ablation plumes has been studied extensively in recent years [1–3]. In this process, coherent [4] short-wavelength radiation is generated through the interaction of an intense femtosecond laser pulse with matter ablated from a surface by a separate laser pulse. Compared to the gaseous atomic nonlinear media (typically the rare gases) usually employed for HHG, ablation plumes allow a very wide range of elements to be studied [3]. Further, by controlling the ablation conditions, neutral atoms and ions can be produced in the plume in their ground-states as well as in electronically excited states. A particularly interesting feature of this process is the observation of resonantly-enhanced coherent radiation which we shall refer to as "resonant harmonics". These resonant harmonics can be enhanced significantly (by up to 2 order of magnitude [1, 2]) compared to neighbouring non-resonant ones. This increased harmonic flux is of potential importance for applications of the radiation, such as coherent diffractive imaging [5] and attosecond pulse generation [6–10].

The resonant enhancement observed when the harmonic frequency is close to that of the transition between the ground state and an autoionizing state (AIS) of the generating species can be understood in terms of a four-step model [11], which is based on the well-known three-step model for HHG in gas atoms [12, 13]. In both models, the first two steps (tunnel ionization, followed by laser-acceleration of the electron in the continuum) are essentially the same. However, in the four-step model, the third step of the three-step process (radiative recombination from the continuum to the ground-state) is replaced by a trapping of the electron in an AIS, followed by a fourth and final step which is a relaxation to the ground state and the emission of a short-wavelength photon. This can occur with higher probability than the three step process due to the large inelastic scattering cross-section governing the trapping in the AIS, and the high oscillator strength of certain ground-AIS transitions.

A generalized theory of HHG [14] based on the four-step model shows that resonant harmonic spectrum, $\mu(\omega)$, can be expressed as

$$\mu(\omega) = \mu_{NR}(\omega) F(\omega) \tag{1}$$

where $F(\omega)$ is the resonant enhancement factor (which is unity far from resonance), and $\mu_{NR}(\omega)$ is the spectrum in the absence of resonances. In this work, we studied relatively low order harmonics (around 13th and 15th order) in the vacuum ultraviolet (VUV), which is of particular interest for pump-probe experiments [15, 16]. In the case of few-cycle drive pulses, $\mu_{NR}(\omega)$ takes the form of broad harmonic peaks in this spectral range [16–18] which can overlap with a number of narrower resonances in the generating medium described by $F(\omega)$.

Optics EXPRESS

This leads to the emission of a spectrum, $\mu(\omega)$, in which resonant lines of highest oscillator strength are picked out where they overlap with $\mu_{NR}(\omega)$. Consequently, the emission lines can be detuned from the center frequencies of the non-resonant harmonic. The influence on the resonant spectrum of the chirp of the drive pulse has been investigated for multi-cycle drive pulses [19–21], but there has been very limited experimental data in the few-cycle regime [22]. In this work, we experimentally studied the chirp dependence of resonant HHG in an indium ablation plume using few-cycle drive pulses (3.5 fs) which are close to the typical lifetime of the AIS involved. Our data are consistent with Eq. (1) showing that this formalism is valid in the few-cycle limit as well. Moreover, our results reveal opportunities for the chirp control of resonant harmonics.

2. Experimental setup

The experimental setup is shown in Fig. 1. A chirped-pulse-amplification (CPA) Ti: sapphire laser (Femtolasers GmbH, Femtopower HE CEP) provided carrier-envelope phase (CEP) stabilized pulses (CEP fluctuations of < 250 mrad rms, from single-shot measurements) of 28 fs duration and energies of up to 2.5 mJ at a repetition rate of 1 kHz. For these experiments, 1 mJ pulses were focused into a 1-m-long differentially pumped hollow core fiber (250 μm inner core diameter) filled with neon, to spectrally broaden the pulses [23–25]. These pulses were then compressed by 10 chirped mirrors (PC70 Ultrafast Innovations GmbH) and a pair of fused-silica wedges (OA124, Femtolaser GmbH) to finely tune the group delay dispersion (GDD). The resulting compressed pulses used for these experiments had a center wavelength of 775 nm, a pulse energy of 0.5 mJ and a near Fourier transform-limited pulse duration of ~3.5 fs (equivalent to 1.4 optical cycles). The pulse duration was measured by a spatially encoded arrangement for spectral shearing interferometry for direct electric field reconstruction (SEA-F-SPIDER) [26].

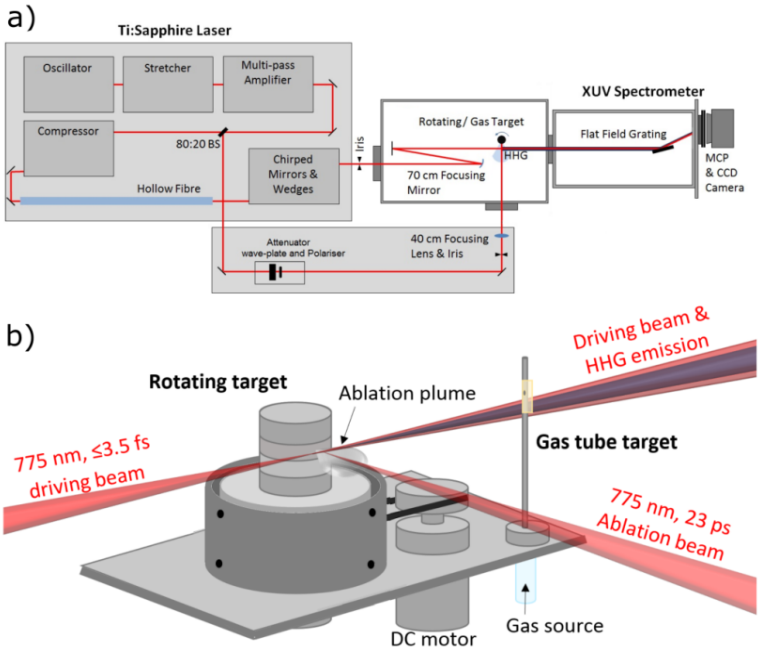

Fig. 1. Experimental setup. (a) Intense few-cycle (~3.5 fs) pulses from a hollow-fiber pulse compressor were used to generate resonant harmonics in an indium ablation plume. The high harmonics were analyzed with an XUV spectrometer as a function of the pulse GDD which was controlled using a pair of wedges. A beamsplitter before the laser compressor was used to obtain synchronised ablation pulses (23 ps duration). (b) The indium plume was produced by

Optics EXPRESS

irradiating a rotating indium rod with the ablation pulses. High harmonics could also be generated in the same beamline by translating into the beam a gas tube target.

To generate high-order harmonics, the few-cycle pulses were directed into a HHG beamline [24] that permits the use of both gas-phase and ablation plume nonlinear media for HHG. The few-cycle pulses were focused with a f = 70 cm concave mirror (confocal parameter $b \approx 10$ mm). The focusing position for the ablation plume target was found by optimising the resonant harmonic signal. It corresponded to focusing the few-cycle pulses just a few mm before the target. Under these conditions, both short and long trajectory contributions to the resonant emission are expected. The indium ablation plume was created by ablating the surface of a rotating indium target with a laser pulse arriving 36 ns [2] before the HHG drive pulse. The ablation laser pulse was obtained by splitting off part of the CPA laser beam before the compression gratings with an 80:20 beamsplitter. The ablation pulse had a center wavelength of 800 nm and a pulse duration of 23 ps. An attenuator comprising a half-waveplate and polarizer permitted the ablation pulse energy on target to be controlled in the range 0-110 μJ. The ablation pulses were focused to a peak intensity of 1.3×10^{11} W/cm^2 onto the indium target with a 40 cm focal length lens. The indium targets (Ktech, 99.9% purity) were 15 mm in diameter and rotated at 30 RPM by a DC motor. Rotating the target considerably improves the stability of the generated harmonics compared with fixed targets in the case of higher pulse repetition rate (1kHz) [27].

The harmonics were analyzed using a spatially-resolving XUV spectrometer with a grazing incidence flat-field grating (1200 lines/mm, Hitachi). The harmonic radiation was detected with an imaging microchannel plate (MCP) detector (Photonis USA, Inc.) read out by a CCD camera (CoolView FDI, Photonic Science). The maximum error in the absolute wavelength calibration in the 15-25 eV range was ≈0.3 eV. Spatially-resolved HHG spectra were recorded for different drive pulse CEP and chirp. To alter the chirp of the drive pulses, one of the fused-silica wedges (2.8° wedge angle) after the hollow fiber was translated through the beam by a computer-controlled motorized stage. In this way the GDD (linear chirp) could be varied. Each 100 μm of fused silica inserted/removed from the beam corresponds to an increase/decrease of the GDD by ~3.5 fs^2. Inserting more/less wedge into the beam compared to the optimal compression position gave positively/negatively chirped pulses respectively. For a linearly chirped Gaussian pulse, the chirped pulse duration is given by

$$\Delta t_{chirped} = \frac{\sqrt{\Delta t_{TL}^4 + 16\ln(2)^2 \phi_2^2}}{\Delta t_{TL}} \tag{2}$$

where Δt_{TL} is the transform-limited (unchirped) pulse duration and ϕ_2 is the GDD. The simulations in Fig. 2 show how the pulse duration and GDD vary as a function of the relative wedge insertion for Δt_{TL} = 3.5 fs. The chirped pulse duration can be seen to increase symmetrically around the zero wedge insertion position. We define the zero position as the wedge position that results in the shortest pulse duration at the ablation plume, with positive/negative insertion resulting in positively/negatively chirped pulses. This position is determined by maximising the high harmonic cut off in neon, which is delivered into the interaction region using the gas target on the combined ablation plume/gas needle apparatus. Numerical examples of unchirped and chirped pulses are shown above the main plot in Fig. 2.

Optics EXPRESS

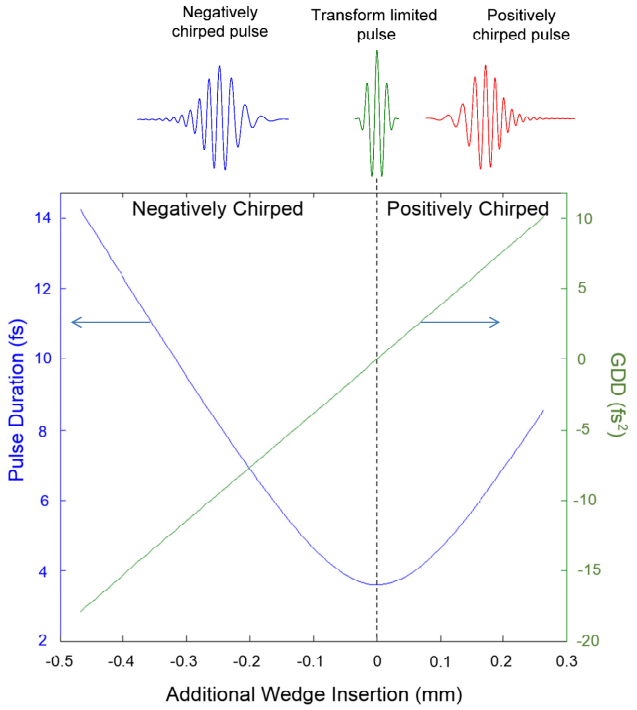

Fig. 2. Simulated examples of pulse chirping. The main plot shows the pulse duration (blue curve, left axis) and GDD (green line, right axis) as a function of wedge insertion into the drive laser beam. The curves were calculated using the known dispersion of fused silica at 775 nm. The wedges are used to fine-tune the GDD after a hollow fiber pulse compressor. The zero wedge insertion position corresponds to the wedge insertion that yields an unchirped 3.5 fs pulse. The electric field waveforms for a negatively chirped (left, blue), unchirped (center, green) and positively chirped (right, red) pulses are shown above the main plot.

Translating the wedges also introduces a change to the CEP of ~4π/100 μm for fused silica wedges at 775 nm. Due to the very short duration of our laser pulses, a 2π change in the CEP achieved by inserting an extra 50 μm of fused silica already broadens our 3.5 fs pulse to almost 4 fs. In this paper we present chirp scans over a relatively large wedge insertion range of ~400 μm, where both the CEP and pulse chirp are varying. This is fully accounted for in our simulations.

3. Experimental results

Figure 3(a) shows the measured HHG spectrum (integrated over a divergence of +/–0.5 mrad) from the indium ablation plume as a function of GDD (bottom axis). The estimated laser pulse duration (assuming that the 0 wedge position corresponds to a 3.5 fs transform limited Gaussian pulse) is shown on the top axis, with positively/negatively chirped pulses to the right/left of the minimum pulse. The peak intensity at the minimum pulse duration position was ~10^{14} W/cm^2 decreasing on either side of this position as the inverse of the pulse duration. The spectrum at each wedge position was integrated over about 10^3 laser pulses. Note that atomic indium, with its low ionization potential (5.8 eV), is ionized on the rising edge of the driving pulse at intensities which are at least an order of magnitude lower than the peak intensity. Low order harmonics which might be generated during atomic indium photoionization are not studied here. On the other hand, doubly-charged indium ions have a much high ionization potential (28 eV) and are not significantly ionized by the laser pulse. So we can conclude that the emission spectrum in the range of 17-25 eV studied in this paper is generated predominantly by singly-charged indium ions.

Optics EXPRESS

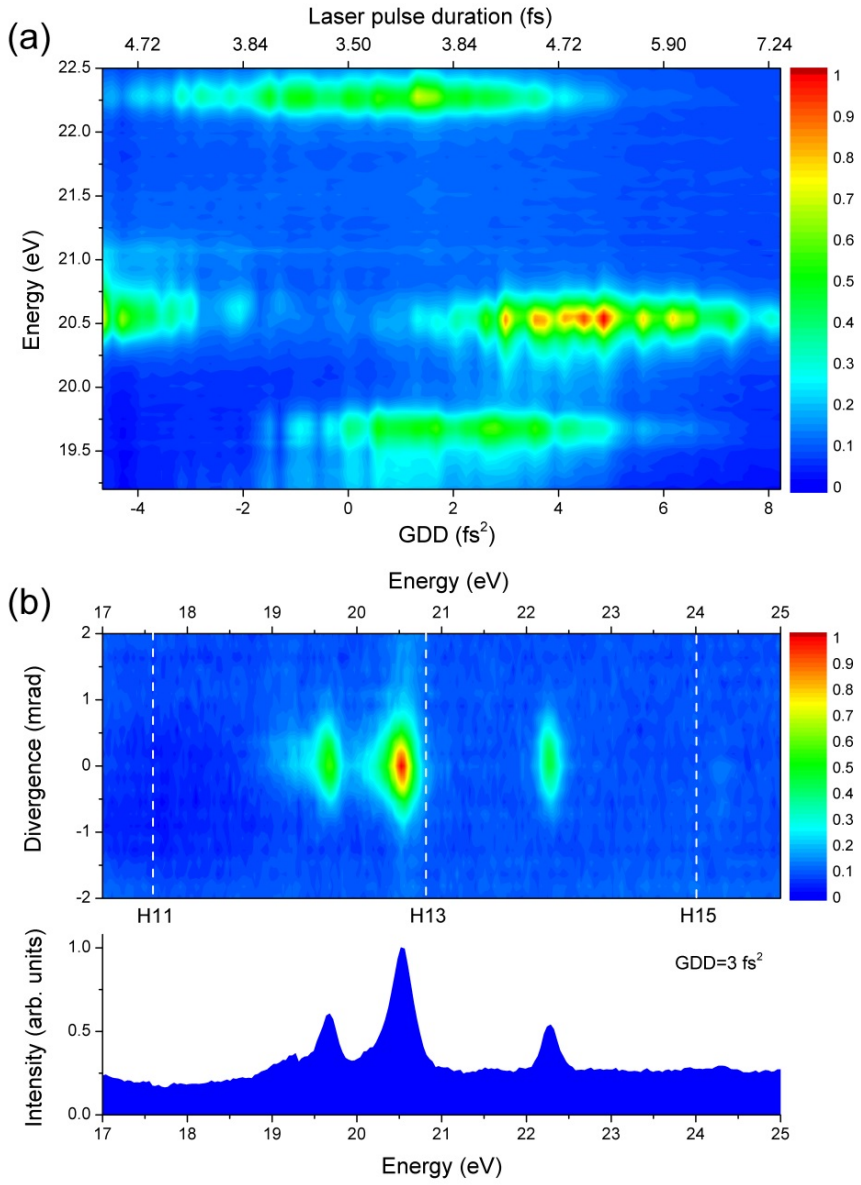

Fig. 3. Experimental data. (a) Measured emission spectrum from the indium ablation plume irradiated by 775 nm pulses as a function of the wedge insertion (GDD) in the drive pulse. The minimum pulse duration was ~3.5 fs at the 0 GDD position. The pulse durations on the top axis are calculated assuming that this corresponds to a Fourier transform limited pulse. Three resonant harmonics are observed at approximately 19.7, 20.5 and 22.3 eV which are maximized at different wedge positions. (b) Spatially-resolved spectrum obtained with the 3 fs^2 of GDD on the drive pulse.

Figure 3(b) shows the spatially-resolved HHG spectrum at the wedge insertion position corresponding to 3 fs^2 GDD, for which all the observed spectral features are prominent. The low beam divergence (FWHM divergence ≈1 mrad) is similar the divergence of high harmonics from a Ne gas target obtained in the same beamline.

Three spectral features are evident at 19.7, 20.5 and 22.3 eV which respond differently as the chirp is changed. As detailed in Table 1, the energies of these features correspond closely

Optics EXPRESS

to transitions between AISs and either the ground state of InII (19.7 eV feature) or an excited state InII* (20.5 and 22.3 eV features) with relatively large oscillator strength [28]. No other spectral features were observed in this energy range under our experimental conditions, even when the MCP voltage was increased to saturate the signal of the three aforementioned lines. These three features are in the vicinity of the 13th (20.8 eV) and 15th harmonic (24.0 eV) of the 775 nm (1.6 eV) pulse.

Table 1. Assignment of the experimentally observed spectral features.

Ion	Transition	Energy theory (eV)	Energy experiment (eV)	*gf*-value theory
InII	$4d^{10}5s^2 \rightarrow 4d^9 5s^2 5p$: $^1S_0 \rightarrow (^2D)\ ^1P_1$	19.92	19.7	1.11
InII*	$4d^{10}5s5p \rightarrow 4d^9 5s5p^2$:			
	$^3P_2 \rightarrow (^1S)\ ^3D_3$	20.53	20.5	0.40
	$^3P_2 \rightarrow (^1D)\ ^3G_3$	21.98	22.3	0.76

Spectroscopic notation is used, e.g. InII refers to the singly charged ion In^+. The theoretical values [28] are derived from multi-configuration Hartree-Fock calculations. The experimental values were obtained using the dual laser plasma technique. A number of closely spaced lines are identified in [28] in the vicinity of 20.5 eV. We have selected the transition with the highest oscillator strength.

The measured chirp dependence of each emission line is asymmetric and shows some complex modulated structure. Within our wedge scan range, each line is enhanced for positively chirped drive pulses, though the 20.5 eV line also shows enhancement for negative chirp.

4. Numerical simulations and discussion

To simulate our experimental results, we numerically solved the three-dimensional time-dependent Schrödinger Eq. (3)D TDSE) for a model ion in the laser field based on the four-step model for HHG [11] using the single-active electron approximation. The potential reproducing the interaction of the active electron with the nucleus and with the rest of electrons was chosen in the form suggested [11]. It can be written as a combination of a soft-core Coulomb potential and the barrier, thus allowing for the quasi-stable state with the positive energy modelling the AIS:

$$V(r) = -\frac{Q+1}{\sqrt{a_0^2 + r^2}} + a_1 \exp\left[-\left(\frac{r-a_2}{a_3}\right)^2\right] \qquad (3)$$

where Q is the charge state of the generating system (in the case of InII (or InII*) it is 1), and a_0, a_1, a_2, a_3 are constants chosen to replicate the properties of the generating system such as the ground state energy (the ionization potential of InII is 18.87 eV), AIS energy and AIS width. The latter is found from the experimental data presented in [24]. Note that for the transition with energy 19.92 eV this width corresponds to the AIS lifetime of 3.3 fs thus close to the duration of our laser pulse (3.5 fs).

Due to the large bandwidth of the few-cycle pulses used in our experiment, the emission spectrum consists of several lines emitted from populated AIS embedded in the continuum. Thus, the generation of the experimentally observed lines can be described within the framework of resonant HHG theory [11, 13]. According to this theory [13], the generation of each line can be considered separately, since the lines are well localized and the energy differences between the adjacent lines are much greater than the linewidths. Hence, we numerically solved the 3D TDSE for each line separately with the parameters for our model potential (Eq. (3)) chosen to match each transition in Table 1.

The modification of an initially transform-limited laser pulse in passing through the wedges can be expressed as

Optics EXPRESS

$$E(\omega) = E_{TL}(\omega, \phi_{CE}) \exp[-i\phi(\omega)] \quad (4)$$

where $E_{TL}(\omega, \phi_{CE})$ is a transform-limited 1.5 cycle sine-squared pulse (the duration of which is the closest to the one used in the experiment) of central wavelength 775 nm and peak intensity of 10^{14} W/cm^2 with CEP = ϕ_{CE}, and spectral phase $\phi(\omega) = n(\omega)\omega L/c$, where $n(\omega)$ is the refractive index of the wedges (fused silica), L the additional material path introduced by the wedges (L = 0 corresponds to wedge position for TL pulses), and c is the speed of light. In the TDSE simulations we used the standard Taylor expansion of the spectral phase up to second order around the central frequency, ω_0, to allow us, for these computationally-expensive calculations, to efficiently cover the relatively broad GDD range used in our experiment:

$$\phi(\omega) = \phi_0 + (\omega - \omega_0)\phi_1 + \tfrac{1}{2}(\omega - \omega_0)^2 \phi_2 \quad (5)$$

where ϕ_0 is a common phase shift, ϕ_1 is the group delay (GD), and ϕ_2 is the GDD. To simulate our wedge scans, we set ϕ_{CE} = 0 (initial cosine waveform with respect to the envelope) and scanned L. As $|L|$ (and hence |GDD|) is increased, the CEP is changed, the pulse becomes linearly chirped and its duration is increased.

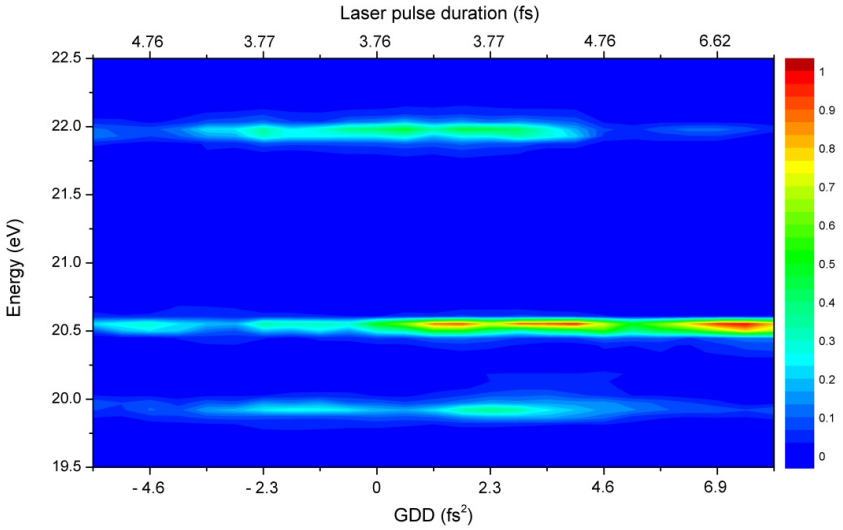

Fig. 4. Simulated emission spectrum as a function of wedge insertion to be compared to the experimental data in Fig. 3(a). The duration and pulse GDD are shown on the top and bottom axes respectively. The intensities of the lines are corrected taking into account *gf*-factors of the transitions (see Table1).

The TDSE simulation results are shown in Fig. 4 for each of the three emission lines. We note that these are single-atom calculations and hence no phase-matching effects are included. In agreement with the experimental results, the calculated chirp dependence is asymmetric with the general trend of stronger emission for positively chirped pulses. A complex modulated structure is also evident. The effect of higher order dispersion terms (not included in our TDSE simulations, though accounted for in our SFA calculations) may account for some of the differences between theory and experiment. To isolate intensity from chirp effects, we carried out separate simulations in which the peak laser intensity was varied for a transform-limited pulse with a constant CEP of duration 3.7 fs. The results are shown in Fig.

Optics EXPRESS

5. The peak laser intensity at each horizontal position in the plot is the same as the chirp scan in Fig. 4 at the same axis position.

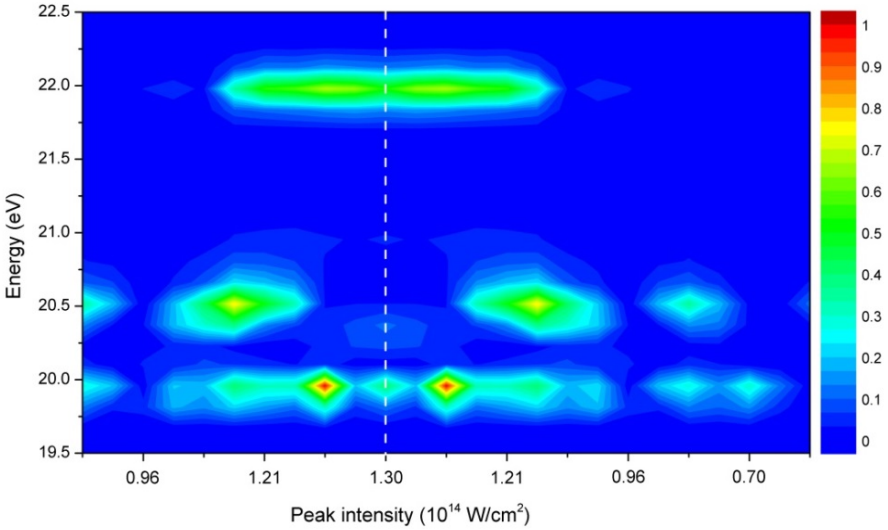

Fig. 5. Simulated emission spectrum as a function of the peak laser intensity for unchirped pulses of 3.7 fs duration. The peak intensity is the same as in Fig. 6. The dashed vertical line marks the position of the maximum intensity ($1.3x10^{14}$ W/cm^2) in this simulated scan. The intensities of the lines are corrected taking into account *gf*-factors of the transitions (see Table1).

It is obvious that, neglecting CEP/chirp effects, the intensity variation arising from the wedge scan would lead to symmetric emission structures around the maximum intensity (white dashed line at $1.3x10^{14}$ W/cm^2). As shown in Fig. 5, for all three lines, there is a local minimum in the emission intensity at the peak drive laser intensity. The asymmetries with respect to the zero GDD position seen in the experimental and full simulated wedge scans are clearly CEP/chirp effects.

A conceptual model for the chirp dependence of resonant harmonics can be developed as follows. It is well-known that the HHG spectrum generated by few-cycle pulses can be quasi-continuous near the spectral cutoff, a result of there being only a single recollision event during the pulse with sufficient energy to produce this radiation [29–31]. However, for lower frequency emission in the HHG plateau (typically in the VUV range, as in this experiment), spectral modulation is pronounced since even for a few cycle drive pulse, several recollisions at consecutive laser half cycles can contribute to the emission. Due to the change of the generating field from one half-cycle to another in the few-cycle pulse, the periodicity of the emission can be different from the half-cycle periodicity typical for a multi-cycle laser pulse. The VUV radiation in a certain spectral range is emitted in a small number of consecutive bursts [32, 33]. The time delay between the bursts is not exactly equal to the laser half-cycle and depends on the VUV frequency, laser pulse CEP [33, 34], chirp [32] and intensity. In the frequency domain the interference of the bursts leads to the modulation of the HHG spectrum, and the periodicity of the modulation is the inverse time delay between the bursts. This results in a complex picture of harmonic interference maxima (“fringes”) as a function of the drive laser chirp.

To simulate these fringes, we have conducted numerical modelling of non-resonant HHG with chirped laser pulses under the strong field approximation (SFA) [35, 36] using the saddle-point method. An integration gate was employed that allowed contribution from both

Optics EXPRESS

short and long trajectories on the first recollision. The ionization potential was set to that of InII (18.87 eV), the laser wavelength was 775 nm, and the transform-limited pulse duration and peak intensity were 4 fs and $1.3\text{x}10^{14}$ W/cm^2, respectively. The material dispersion of the wedges was treated to all orders by using a Sellmeier expression for the refractive index of fused silica. The chirped pulses were modelled as in the TDSE simulations described above. Intensity averaging [37] was used to simulate macroscopic propagation. This involves coherently summing the time-dependent dipole over an appropriate range of intensities to model the laser intensity variation within the interaction volume. The results are shown in Fig. 6. A complex interference pattern is observed, which even in the absence of ionization [38] shows a chirp asymmetry. Overlaid are the three indium resonant frequencies that were used in our TDSE simulations.

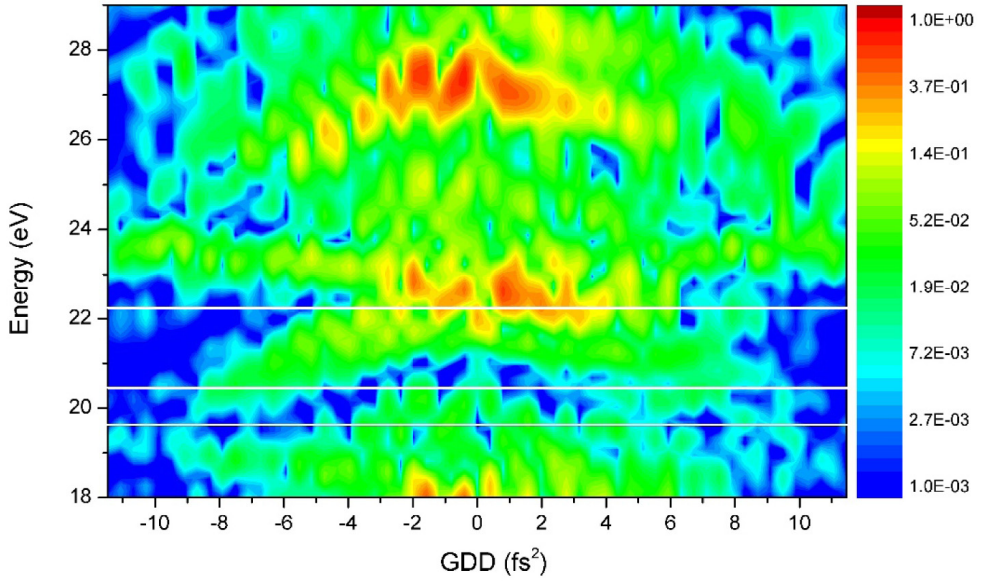

Fig. 6. SFA simulation of non-resonant HHG with chirped laser pulses following propagation through a fused silica wedge pair. A logarithmic intensity scale has been used to highlight the complex modulations in signal intensity. The three horizontal lines correspond to the experimental frequencies of the indium resonance lines at 19.7eV, 20.5 eV and 22.3 eV.

The theory of resonant HHG [14] predicts (see Eq. (1)) that the conditions for which the emission is resonantly enhanced in a wedge-scan can be understood as the intersection of the non-resonant fringe pattern and the resonant frequencies in Fig. 6. In Fig. 7(c) we use Eq. (1) to plot the resonant behavior. To aid comparison with the experimental data, the resonant factors $F(\omega)$ were set to arbitrary values to ensure equal maximum signal levels for each resonant line, and with widths approximately matching the experimental widths.

Optics EXPRESS

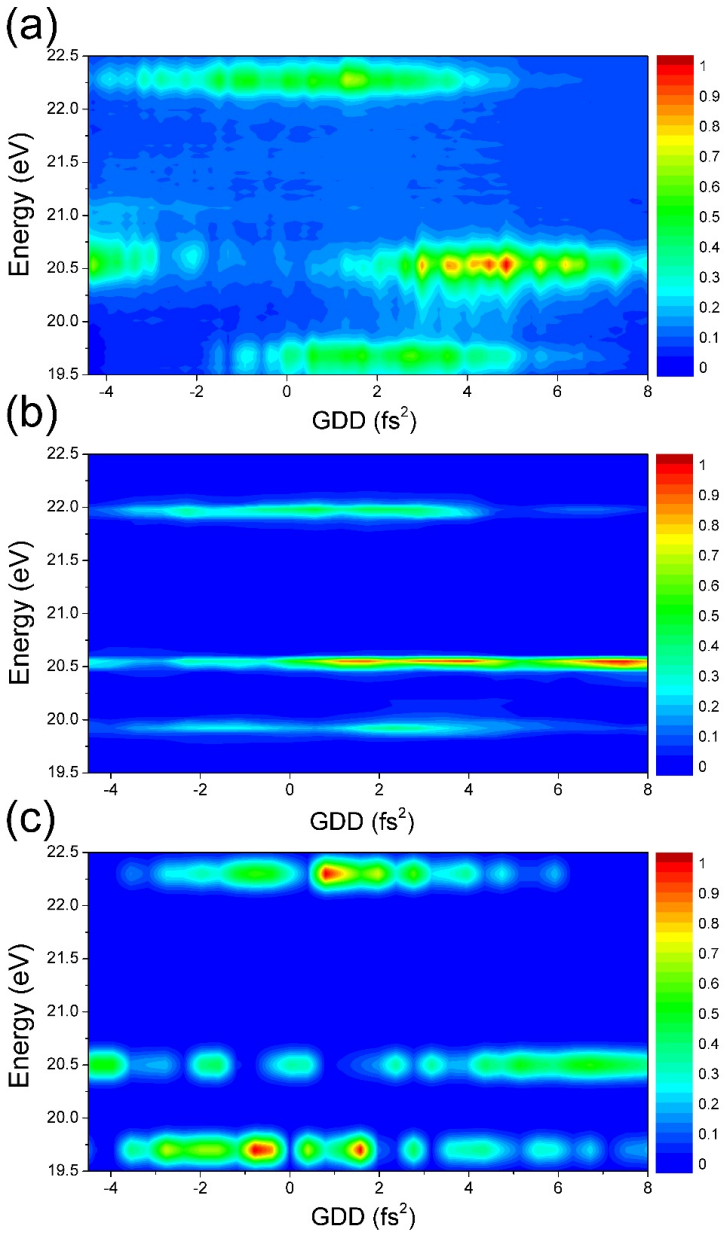

Fig. 7. Comparison of experimental data and simulations. (a) Experimental data, (b) TDSE calculations, (c) product of non-resonant SFA simulations and resonant factors. Note that in (b) and (c) the theoretical resonant frequencies were used from Table 1.

The radiation measured in our experiments arises from both microscopic (single emitter) and macroscopic (propagation) effects. To estimate the relative importance of propagation effects, we first consider phase-matching with coherence length, $L_{coh} = \pi/\Delta k$, where Δk is the wave vector-mismatch. In our experiments we used relatively loose focusing (b ≈10 mm) and a thin target (L_{med} ≈0.1 mm) and hence we can neglect the geometric contribution to Δk. We can also ignore the ionic contribution to the refractive index (RI) change for the fundamental, and the electron contribution to the change in RI for the VUV emission. Hence,

Optics EXPRESS

the wave vector-mismatch can be written $\Delta k \approx \frac{\omega}{c}\left(\Delta n_{\omega}^{(ions)} - \Delta n_{0}^{(elecs)}\right)$, where $\Delta n_{\omega}^{(ions)}$ is the RI change for the emitted radiation due to ions [22] and $\Delta n_{0}^{(elecs)}$ is the RI change for the fundamental due to free electrons. Based on similar experiments, e.g [39], we estimate our target density to be $1\text{x}10^{17}$ cm^{-3} (or likely less) which we take to be both the InII and free electron densities. The maximum value of $\Delta n_{\omega}^{(ions)}$ is achieved near the resonance. Calculating this maximum value using parameters of the 19.92 eV transition (the one with the highest oscillator strength) from [28] we find that for our conditions $\left|\frac{\Delta n_{o}^{(elec)}}{\Delta n_{\omega}^{(ions)}}\right| > 4$. Thus, the dominant contribution to the phase-matching is due to the free electrons. The coherence length for the frequencies near the resonance for these conditions is found to be approximately 1 mm. Therefore $L_{coh}/L_{med} > 10$, and we can conclude that the resonant emission spectrum is not significantly modified by phase-matching. The absorption of the generated radiation, with absorption length Labs near the resonance could also be important. However, we estimate that for our conditions that $L_{abs}^{(\min)}/L_{med} > 5$ and hence the observed spectrum is not changed significantly by absorption. Overall, we can thus conclude that propagation effects are not important in shaping the measured spectrum and that single-emitter simulations should be sufficient to capture the main features of the experimental data.

Qualitative agreement of the theoretically obtained results with the experiment data is obtained. It becomes apparent that the experimentally observed structures that are asymmetric with laser chirp, as well as the minima for zero chirp, arise from the intersection of the resonant frequencies and the asymmetric chevron-like non-resonant HHG intensity pattern.

5. Conclusions

In conclusion, we have experimentally studied the effect of laser chirp on VUV (around 20 eV) resonant high harmonics generated in an indium ablation plume by few-cycle pulses with a center wavelength of 775 nm. We find that the resonant emission shows a strong chirp dependence, with pronounced modulations and an asymmetry with regard to the sign of chirp. We have numerically simulated the single-particle response by solving the 3D TDSE for the model ion having quasi-stable state. The simulations reproduce qualitatively the main features of the data, in particular the positive/negative chirp asymmetry and modulated resonant emission structure as a function of GDD. We also carried out TDSE calculation where only the intensity of the pulse was changed. These show that the observed chirp dependence cannot be attributed to changes in the peak laser intensity alone. Separately, we performed SFA simulations of HHG as a function of laser chirp using intensity averaging. The SFA results show a complex harmonic intensity distribution. The overlap of the resonant lines' photon-energies with this distribution, as described in the theory of resonant HHG, picks out a resonant emission spectrum which is in good agreement with the experimental data. This work thus provides, to the best of our knowledge, the first experimental verification of the resonant HHG theory in the few-cycle limit. Furthermore, the ability to control the resonant emission by making relatively small changes to the chirp of the drive pulse provides a straightforward way to control the relative intensities of different coherent emission lines. In some cases, it should be possible to effectively switch lines on or off using the laser chirp. Through careful choice of the ablation target, the photon energies of these ultrafast pulses could be tailored for a particular application, for example in pump-probe studies.

Optics EXPRESS

Funding

EPSRC (EP/I032517/1, EP/J002348/1); EPSRC/DSTL (MURI EP/N018680/1); The Royal Society (NF161013, IE130323), Marie Sklodowska-Curie Innovative Training Network (HICONO); Russian Science Foundation (Grant No. 16-12-10279).

Acknowledgments

We would like to thank Dr. Emilio Pisanty for helpful discussions, and Mr. A. Gregory and Mrs. S. Parker for their technical assistance. Numerical TDSE studies were supported by the Russian Science Foundation (Grant No. 16-12-10279).